Determination of triple points in the phase diagram of praseodymium

Y. C. Zhao,* F. Porsch, and W. B. Holzapfel

Fachbereich Physik, Universität-GH-Paderborn, D-33095 Paderborn, Germany
(Received 25 January 1995)

The phase diagram for praseodymium under pressures up to 23 GPa and temperatures up to 573 K is studied by *in situ* energy-dispersive x-ray diffraction with an externally heated diamond-anvil cell apparatus along the phase boundaries between Pr(II) (fcc), Pr(III) (distorted fcc), and Pr(IV) (α-uranium-type structure). The triple point of these three phases is located around 21 GPa and 537 K, representing the end point of the apparently second-order phase transition between Pr(II) and Pr(III) at the transition to the high-pressure phase Pr(IV). Together with the compression data for Pr at ambient temperature, the present study extends the P-T phase diagram up to the melting lines.

The structural systematics of the regular trivalent lanthanide (Ln) metals (from La to Lu without Ce, Eu, and Yb) have been studied near ambient pressures in a wide range of temperatures and under higher pressures in more restricted temperature ranges.[1-9] After Ce, Pr is the next Ln metal which shows strong $4f$-electron contributions to its structural energy under pressure, manifested by the volume-collapse transition from Pr(III) (distorted fcc) to Pr(IV) (α-U-type structure) and by similarity in its resistivity behavior at the Pr(III)-Pr(IV) transition around 21 GPa in comparison with the γ-α phase transition of Ce,[6,9-11] which is generally related to $4f$-electron delocalization. The boundaries in the P-T phase diagram for Pr had been studied earlier by differential thermal analysis,[12,13] x-ray diffraction,[7] and at low temperatures by electrical resistivity measurements. Especially the results[9,14] on the Pr(II)-Pr(III) and Pr(III)-Pr(IV) boundaries gave hints for the possible existence of a new triple point. The primary intention of the present work was the search for this triple point, keeping in mind that the transition between Pr(II) with its fcc structure and Pr(III) with its distorted-fcc structure has been considered to be an apparently second-order phase transition, which could result in a special triple point at the strong first-order phase transitions[5-8,15,16] to Pr(IV).

In addition, the unusually flat melting curve for Pr(II) and some discrepancy with shock-wave data on melting under pressure raised the question as how these results could be reconciled with the existence of the high-pressure phase Pr(IV) and with the indications of $4f$-electron delocalization.

In the present measurements, pressure was generated with a diamond anvil cell (DAC).[17,18] An external electrical resistivity heater was used to obtain homogenous temperatures in the sample up to 573 K. The phases were identified by energy-dispersive x-ray diffraction (EDXD) with a tungsten fine-focus x-ray tube operated at 25 mA and 60 kV and a conical collimator system with $2\theta \approx 10°$ placed in front of a large-area intrinsic Ge detector as described previously.[19] The exact value of 2θ in each run was calibrated by EDXD spectra of gold powder. This system is especially suitable for high-pressure–high-temperature EDXD studies due to the averaging over the whole diffraction ring, which improves the spectral quality for coarse-grained samples significantly. Mineral oil was used as the pressure-transmitting medium to prevent also the sample from oxidation during sample loading. This oil is obviously chemically inert to Pr up to at least 573 K, because no spurious diffraction peaks could be detected. With the present experimental instrumentation, diffraction spectra recorded in less than 100 s have sufficient intensity to analyze the phase composition. The Pr sample material had been obtained from K. A. Gschneidner, Jr., with analysis of the major impurities in atomic ppm: 652 for oxygen, 23 for iron, and 17 for other rare metals.

To locate the phase boundaries, the x-ray-diffraction spectra were recorded either on heating and cooling at fixed load, starting with a defined pressure at room temperature, or by isothermal compression and decompression. In total, 69 EDXD spectra were recorded in these experiments. The temperatures were measured and controlled by a PID regulator with a calibrated Chromel-Alumel thermocouple in contact to one diamond anvil. The pressures were measured at room temperature by the ruby fluorescence technique.[20] At the higher temperatures the fluorescence signal of ruby R lines became too weak for accurate pressure determinations. Since the diffraction spectra of the common pressure standards for high-temperature x-ray measurements such as Au and Pt (Refs. 21 and 22) interfere seriously with the spectra of the sample, no extra internal pressure standards were used, but the pressures at elevated temperatures were evaluated directly from the measured volume of the Pr sample itself, taking into account that the thermal correction could be estimated with sufficient accuracy by the equation of state. From the 300-K isotherm[6] with a Debye temperature[23] $\Theta_D = 151$ K, the approximation $\gamma / V = \gamma_0 / V_0$, and a Slater-Grüneisen parameter[24] $\gamma_{S,0} = 0.83$, the maximum thermal pressure correction is only 0.5 GPa (at 21 GPa and 573 K). Runs in the processes of heating and cooling at a fixed load indicated that the pressures evaluated by the above method were very close to the corresponding starting pressures at room temperature, with the maximum deviations of 0.3 GPa in the lower-pressure range (5–16 GPa) and 0.4 GPa

in the upper range (17–23 GPa) and thus typically within the general experimental uncertainty. This indicates that these heating cycles at a fixed load can be regarded as isobaric processes. The present experimental data on the phase diagram of Pr are represented in Fig. 1 together with earlier results.[7,9,12–14,25] The data[14] for the Pr(III)-Pr(IV) phase boundary below 300 K were shifted by 10% to higher pressures to take into account the later revision[9] of the corresponding pressure determinations.

The Pr(II)-Pr(III) phase boundary was determined primarily in isobaric temperature scans, and Fig. 2 shows typical EDXD spectra at 12.3 GPa, for Pr(III) at 300 K and for Pr(II) at 403 K, respectively, with an indexing of the superlattice diffraction lines by half-integer numbers. It can be seen that the intensities of the superlattice diffraction lines decrease with increasing temperature, and thus the temperature at which these diffraction lines disappear was taken as the temperature of the transition between Pr(II) and Pr(III). The question of whether this phase transition is truly second order, however, could not be resolved with this technique.[16] Since the present EDXD setup, optimized for stronger intensities, does not resolve the $(\frac{3}{2},\frac{1}{2},\frac{1}{2})$ peak from its much stronger (111) neighbor and leads also to an overlap of the $(\frac{3}{2},\frac{3}{2},\frac{1}{2})$ peak with the fluorescence $K\alpha$ peak at higher pressures, the transition temperatures were determined by fitting two Gaussian profiles and a linear background to the (220)-

FIG. 2. Diffraction spectra for (a) Pr(III) at 300 K and (b) Pr(II) at 403 K at 12.3 GPa. The enlarged sections of these spectra on the right side illustrate the intensity variation of the superlattice reflections.

$(\frac{5}{2},\frac{3}{2},\frac{1}{2})$ pair, keeping the full width at half maximum (FWHM) of the Gaussian profiles fixed to their 300-K values. Figure 3 shows a typical variation of the intensity of these two lines with temperature, where both intensities were normalized with respect to the intensity of the $K\beta$ doublet. From the decrease in the intensity of the $(\frac{5}{2},\frac{3}{2},\frac{1}{2})$ peak, one finds at this pressure of 15.2 GPa a transition temperature of 435(15) K. The same method was used for determining the transition temperatures at other pressures, and the results are shown in Fig. 1 by solid circles.

The phase boundary between Pr(III) and Pr(IV) was determined both in isothermal and isobaric scans. Figure 4 shows typical diffraction spectra for the Pr(IV)→Pr(III) transformation under isothermal decompression. Figure 5 presents diffraction spectra for
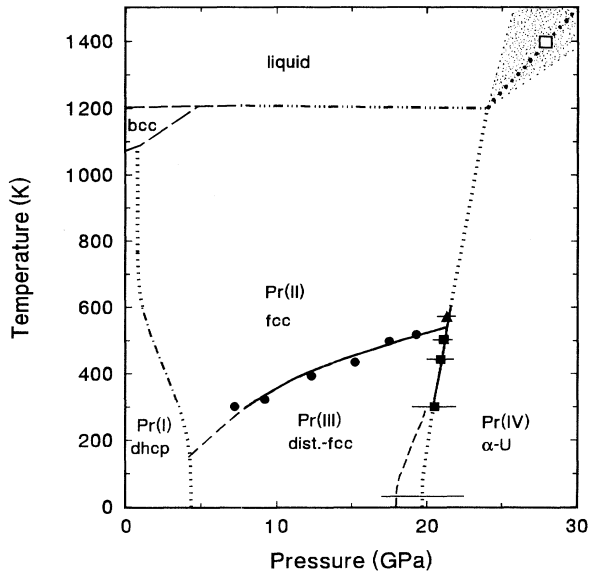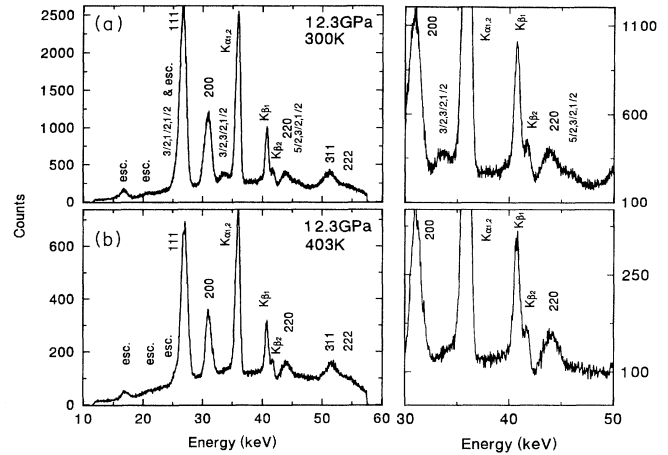

FIG. 1. Pressure-temperature phase diagram of Pr. The present data are represented by solid symbols with the solid lines as guides to eye. The dot-dashed line is from Ref. 7. The long-dashed lines are from Refs. 12 and 13. The triple-dotted–dashed line reproduces the calculated melting line from shock wave data (Ref. 25). The short-dashed lines are from Heinrichs and Wittig (Ref. 14) and Wittig (Ref. 9) with appropriate corrections discussed in the text. A Hugoniot melting point from the shock wave data (Ref. 25) is represented by the open square and dotted lines represent extrapolations and estimates as discussed in the text.
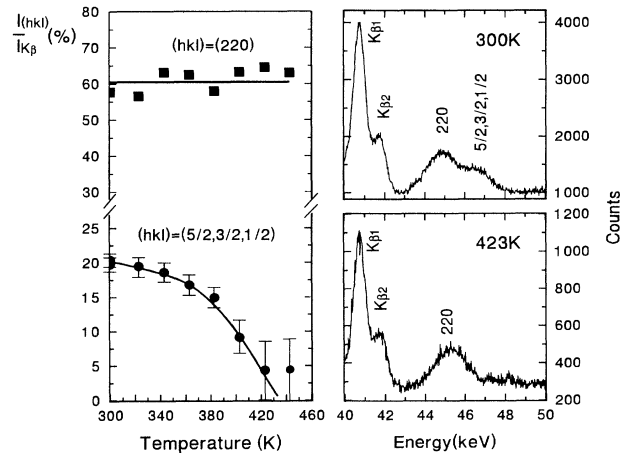

FIG. 3. Typical variation of scaled intensities with temperature at 15.2 GPa. The two spectra at this pressure illustrate the intensity variation of the $(\frac{5}{2},\frac{3}{2},\frac{1}{2})$ peak.

the transformation from Pr(III) (metastable at 300 K and 21.9 GPa) to Pr(IV) at an isobaric 21.9-GPa scan from 300 to 325 K. In contrast to the apparently continuous Pr(II)-Pr(III) phase transition, considerable hysteresis was observed in the Pr(III)→Pr(IV) transformation, where the equilibrium phase transition pressures were taken therefore as the midpoints between the forward and backward transformations at constant temperature T. These data are illustrated in Fig. 1 by solid squares with horizontal lines indicating the width of the hysteresis loop.

One data point for the Pr(II)-Pr(IV) transition measured at 573 K is also shown in Fig. 1 by a solid triangle. An EDXD spectrum for Pr(II) around this data point is shown in Fig. 6. The extrapolation of the II-III boundary toward the stability area of Pr(IV) locates the triple point at 21(1) GPa and 537(15) K. Since the phase transitions Pr(III)-Pr(IV) and Pr(II)-Pr(IV) are strongly first order and the Pr(II)-Pr(III) is apparently of second order, it follows from the Clausius-Clapeyron equation that both the II-IV and III-IV transition lines must have (apparently) the same slopes at the triple point; i.e., there is no kink. The same reasoning applies to the I-II-III triple point.

In addition to the earlier estimates[25] of the melting line for Pr(II), one can use also for Pr(IV) the Lindemann melting relation[26] with the Debye-Grüneisen parameter γ and its estimate from isothermal compression data with $V(\partial^2 P/\partial V^2)/(\partial P/\partial V)=K'_T$ and the Dugdale-MacDonald relation $\gamma=(K'_T-1)/2$ to derive the relation
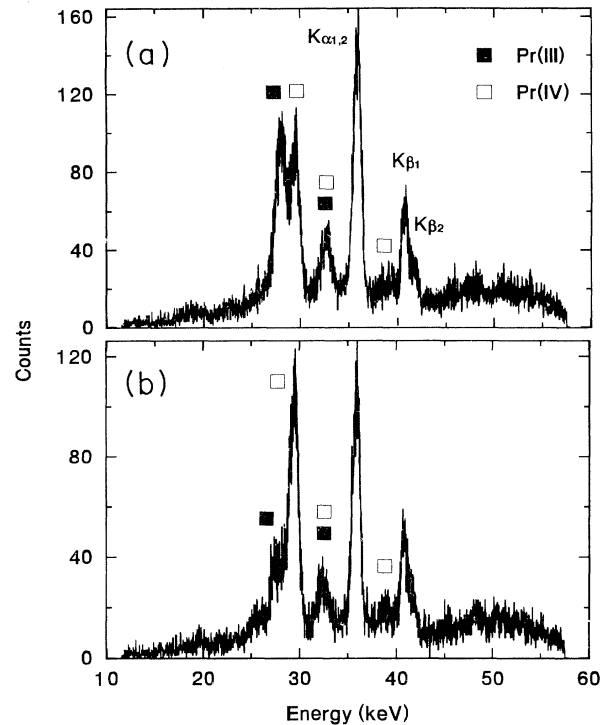

FIG. 5. Diffraction spectra in an isobaric scan at 21.9 GPa for the Pr(III)→Pr(IV) transformation at 325 K with typical acquisition times of 100 s. (a) and (b) are the spectrum for this transition during first 100 and 300 s, respectively.
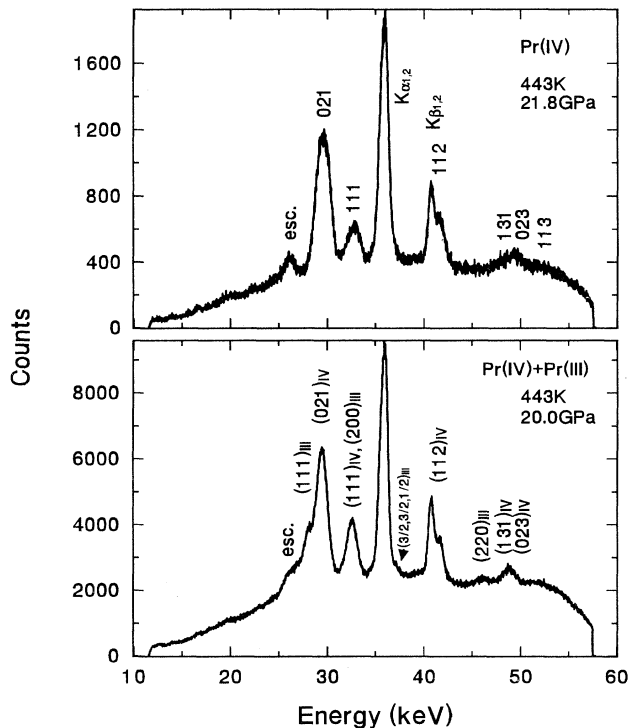

FIG. 4. Diffraction spectra for the isothermal Pr(IV)→Pr(III) transformation at 443 K taken on decompression from 21.8 to 20.0 GPa. Acquisition times are 3 h for the first and 14 h for the second spectrum, respectively.

$dT_m/dP=T_m(2\gamma-\frac{2}{3})/K_T=T_m(K'_T-\frac{5}{3})/K_T$. This relation reproduces the very small slope for the melting line of Pr(II), when one inserts the respective value[6] of $K'_T=2$, and one calculates a significantly larger slope for the melting curve of Pr(IV) when the corresponding values[6] of $K'_T=5$ and $K_T=120$ GPa are taken into account. Since the value for K_T at melting may be somewhat
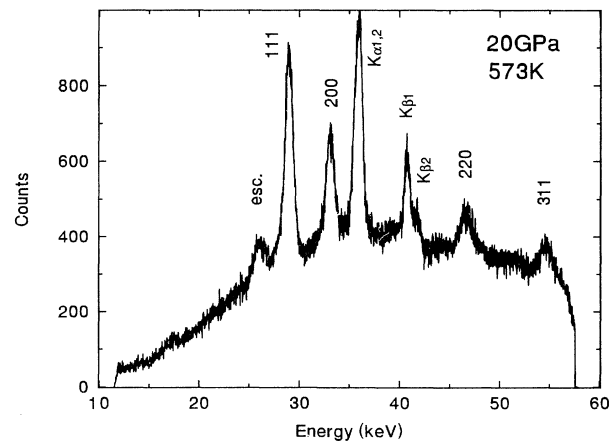

FIG. 6. Diffraction spectrum at 573 K and 20 GPa with the escape peak from the $K\alpha$ lines denoted by "esc" and indexing of the diffraction lines according to the fcc structure of Pr(II).

lower, this slope represents a lower limit for the melting line of Pr(IV). On the other hand, one can also use the Clausius-Clapeyron relation $dT/dP = \Delta V/\Delta S$ for both sections of the melting curve. The measurements show that value of $\Delta V/V$ for the Pr(III)$\rightarrow$Pr(IV) phase transition decreases from 13% at ambient temperature to 7% at 573 K. Therefore $\Delta V/V = 13\%$ gives an upper limit of the volume change at high temperatures. Since $\Delta S_{\text{melting}}$ for both sections of the melting curve can be regarded as being almost constant $\Delta S_{\text{melting}} \sim R$ and large compared with $\Delta S_{\text{II-IV}}$ for the II-IV transition near the triple point, the Clausius-Clapeyron relation results in an increase in the slope of the melting curve at the triple point from almost 0 to about 170 K/GPa, which is considered as an upper limit for the slope of this melting line. Shock wave studies[25] on Ln metals located the melting point on the Hugoniot curve for Pr around 28 GPa and 1400 K as shown in Fig. 1 by an open square, and it was noted[25] that this value for the melting temperature was much higher than their calculated melting line shown as the

triple-dotted–dashed line in Fig. 1. The present study offers an explanation for this apparent discrepancy by the observation that the Hugoniot curve may intercept through the phase Pr(IV) with its much steeper melting curve. The connection between the triple point and the Hugoniot melting point is shown in Fig. 1 by a dotted line, which represents the present best data for melting of Pr(IV) right in the middle between the estimated lower and upper limits.

In summary, one observes a topology of the P-T phase diagram for Pr, which shows a strong similarity to the phase diagram[26] of Ce in its region of the $4f$ delocalization.

---

*Permanent address: Beijing Synchrotron Radiation Facility, Institute of High Energy Physics, Beijing 100039, China.

[1] A. Jayaraman and R. C. Sherwood, Phys. Rev. Lett. **12**, 22 (1964).

[2] D. B. McWhan and W. L. Bond, Rev. Sci. Instrum. **35**, 626 (1964).

[3] G. J. Piermarini and C. E. Weir, Science **144**, 69 (1964).

[4] K. A. Gschneidner, Jr. and F. W. Calderwood, in *Handbook on the Physics and Chemistry of Rare Earths*, edited by K. A. Gschneidner, Jr. and L. Eyring (North-Holland, Amsterdam, 1986), Vol. 8, p. 1.

[5] U. Benedict, W. A. Grosshans, and W. B. Holzapfel, Physica **144B**, 14 (1986).

[6] W. A. Grosshans, Ph.D. thesis, University of Paderborn, 1987; W. A. Grosshans and W. B. Holzapfel, Phys. Rev. B **45**, 5171 (1992).

[7] T. Krüger, B. Merkau, W. A. Grosshans, and W. B. Holzapfel, High Press. Res. **2**, 193 (1990).

[8] U. Benedict and W. B. Holzapfel, in *Handbook on the Physics and Chemistry of Rare Earths*, edited by K. A. Gschneidner, Jr., L. Eyring, G. H. Lander, and G. R. Choppin (North-Holland, Amsterdam, 1993), Vol. 17, p. 245.

[9] J. Wittig, in *Physics of Solids under High Pressure*, edited by J. S. Schilling and R. N. Shelton (North-Holland, Amsterdam, 1981), p. 283.

[10] H. K. Mao, R. M. Hazen, P. M. Bell, and J. Wittig, J. Appl. Phys. **52**, 4572 (1981).

[11] G. S. Smith and J. Akella, Phys. Lett. **105A**, 132 (1984).

[12] A. J. Jayaraman, Phys. Rev. **139**, A690 (1965).

[13] D. R. Stephens, Phys. Chem. Solids **26**, 943 (1965).

[14] M. Heinrichs and J. Wittig, J. Phys. (Paris) Colloq. **39**, C16-1072 (1978).

[15] N. Hamaya, Y. Sakamoto, H. Fujihisa, Y. Fujii, K. Takemu-ra, T. Kikegawa, and O. Shimomura, J. Phys. Condens. Matter **5**, L369 (1993).

[16] F. Porsch and W. B. Holzapfel, Phys. Rev. B **50**, 16212 (1994).

[17] K. Syassen and W. B. Holzapfel, Europhys. Conf. Abstr. **1A**, 75 (1975).

[18] W. B. Holzapfel, in *High Pressure Chemistry*, edited by H. Kelm (Reidel, Boston, 1978), p. 177.

[19] W. B. Holzapfel and W. May, in *High-Pressure Research in Geophysics*, edited by S. Akimoto and M. H. Manghnani (Center for Academic Publication Japan, Tokyo, and Reidel, Dordrecht, 1982), p. 73.

[20] H. K. Mao, P. Bell, J. W. Shaner, and D. J. Steinberg, J. Appl. Phys. **49**, 3276 (1978).

[21] J. C. Jamieson, J. N. Fritz, and M. H. Manghnani, in Ref. 19, p. 27.

[22] L. C. Ming, M. H. Manghnani, J. Balogh, S. B. Qadri, E. F. Skelton, and J. C. Jamieson, J. Appl. Phys. **54**, 4390 (1983).

[23] T. E. Scott, in *Handbook on the Physics and Chemistry of Rare Earths*, edited by K. A. Gschneidner, Jr. and L. Eyring (North-Holland, Amsterdam, 1978), Vol. 1, Chap. 8, p. 591.

[24] The Slater Grüneisen parameter $\gamma_{S,0} = K'_0/2 - \frac{1}{6} = 0.83$ was derived from the value of the isothermal bulk modulus $K'_0 = 2$ given by Ref. 8. The thermal Grüneisen parameter $\gamma_{th,0} = 0.34$ was given in W. J. Cater, J. N. Fritz, S. P. Marsh, and R. G. McQueen, J. Phys. Chem. Solids **36**, 741 (1975). The Dugdale-MacDonald's $\gamma_{DM,0} = 0.45$ was given in W. H. Gust and E. B. Royce, Phys. Rev. B **8**, 3595 (1973). These values of $\gamma_{th,0}$, $\gamma_{S,0}$, and $\gamma_{DM,0}$ all result in small thermal corrections in pressure.

[25] W. J. Cater, J. N. Fritz, S. P. Marsh, and R. G. McQueen, J. Phys. Chem. Solids **36**, 741 (1975).

[26] D. A. Young, *Phase Diagrams of the Elements* (University of California Press, Berkeley, 1990).